JOURNAL OF GEOPHYSICAL RESEARCH, VOL. 105, NO. D20, PAGES 24,849–24,861, OCTOBER 27, 2000

Artificial neural network estimation of rainfall intensity from radar observations

Stefano Orlandini

Dipartimento di Ingegneria, Università degli Studi di Ferrara, Ferrara, Italy

Isabella Morlini

Dipartimento di Economia, Sezione Statistica, Università degli Studi di Parma, Parma, Italy

Abstract. Volumetric scans of radar reflectivity Z and gage measurements of rainfall intensity R are used to explore the capabilities of three artificial neural networks to identify and reproduce the functional relationship between Z and R. The three networks are a multilayer perceptron, a Bayesian network, and a radial basis function network. For each of them, numerical experiments are conducted incorporating in the network inputs different descriptions of the space-time variability of Z. Space variability refers to the observations of Z along the vertical atmospheric profile, at 11 constant altitude plan position indicator levels, namely $\mathbf{Z}^T = (Z_1, \cdots, Z_{11})$. Time variability refers to the observations of $\mathbf{Z}$ at the time intervals prior to that for which the estimate of R is provided. Space variability is evaluated by performing a principal component analysis over standardized values of $\mathbf{Z}$, namely $\tilde{\mathbf{Z}}$, and the first two principal components of $\tilde{\mathbf{Z}}$ (which describe 91% of the original variance) are used to synthesize the elements of $\mathbf{Z}$ into fewer orthogonal inputs for the networks. Network predictions significantly improve when the models are trained with the two principal components of $\tilde{\mathbf{Z}}$ with respect to the case in which only Z_1 is used. Increasing the time horizon further improves the performances of the Bayesian network but is found to worsen the performances of the other two networks.

1. Introduction

Detailed descriptions in space and time of the major rainfall events that produce high rainfall intensities and/or high cumulative rainfall depths are required for both the scientific investigation and the operational control of many hydrological and erosional processes [*Troutman*, 1983]. This provides hydrologists and land users with a relevant challenge, due to the tremendous variability that rainfall displays over a wide range of scales both in space and in time [*Georgakakos and Kavvas*, 1987]. Storm precipitations offer particular observational difficulties as they may incorporate intense convective cells generating high rainfall intensities at scales of 1 km or less, which are not captured well even by high-density rain gage networks [*Chagnon and Vogel*, 1981]. The present generation of weather radars provides an attractive source of information that can be combined with that available from sparse rain gage networks to capture details on storm evolution and rainfall fields at the land surface [*Brandes*, 1975]. Radars provide volumetric observations of the atmospheric reflectivity over large areas ($\sim 10^5$ km^2) with high resolution in space ($\sim$1–2 km) and time ($\sim$5–15 min). The estimation of rainfall intensity at the land surface R from observations of radar reflectivity Z is complicated by several factors that relate to the radar itself (e.g., signal attenuation through a wet radome and beam broadening with distance), to the complexity of the atmospheric processes (e.g., variable of raindrop spectra, anomalous backscattering of melting layer particles, growth and evaporation of precipitation before reaching the ground), and to the radar operation over rugged terrains (e.g., variable ground clutter return and beam blocking) [*Battan*, 1973; *Wilson and Brandes*, 1979]. In addition, scale problems in the radar-gage comparison and errors in rain gage measurements further complicate the identification of the correct relationship between Z and R [*Zawadzki*, 1975; *Hanna*, 1995; *Steiner et al.*, 1999]. On the one hand, detailed physically based analyses of the above mentioned factors are especially important for improving the comprehension of the essential processes that determine the relationship between Z and R [*Austin*, 1987; *Joss and Lee*, 1995; *Andrieu and Creutin*, 1995; *Nešpor and Sevruk*, 1999]. On the other hand, statistical methods may result particularly efficient to produce the most reliable estimates of R from large amounts of observations of Z [*Krajewski and Smith*, 1991].

In the present paper the capabilities of three artificial neural networks (ANNs) to identify and reproduce the relationship between radar reflectivity data along the vertical atmospheric profile and rainfall intensity at the land surface are explored. The importance of incorporating the entire vertical profile of Z to improve the estimates of R has been recognized in several works [*Joss and Pittini*, 1991; *Joss and Lee*, 1995; *Andrieu et al.*, 1995]. The main advantages offered by ANNs with re-

Paper number 2000JD900408.
0148-0227/00/2000JD900408$09.00

spect to other statistical methods are connected to their capability to allow nonlinear processing of distributed representations of the available information and to filter the effects of noise, bias, and outliers in the data set. These capabilities have been proven in many applications, especially where a complex nonlinear mapping must be learned from a massive amount of data affected by measurement errors, such as the task addressed in this work. However, in the application of ANNs, caution must be exercised to use the optimal parameterization for the available data set and to capture the essential underlying processes of interest without fitting too much the noise of the training data [*Bishop*, 1995; *Ripley*, 1996]. The idea of developing an ANN-based algorithm for rainfall estimation using radar observations has been proposed by *Xiao and Chandrasekar* [1997]. The aim of the present work is to provide new statistical insights on the optimal use of radar reflectivity data for the ANN estimation of rainfall intensity at the land surface. The developed methodology is tested using a real data set of reflectivity observed by the Monte Grande radar (Teolo, Italy) and rainfall intensity measured at five rain gage stations in the Cortina d'Ampezzo area (eastern Italian Alps), during the June 12, 1997, storm event.

2. Problem Statement and Solution Methodology

2.1. Radar Rainfall Estimation

Radars are composed of a transmitter, an antenna, and a receiver. The transmitter generates short pulses of energy in the radio-frequency portion of the electromagnetic spectrum. These are focused by the antenna into a narrow beam. They propagate outward at approximately the speed of light. If the pulses intercept an object with different refractive characteristics from air, a current is induced in the object which perturbs the pulse and causes some of the energy to be scattered. Part of the scattered energy will generally be directed back toward the antenna, and if this backscattered component is sufficiently large, it will be detected by the receiver. Measures of the range and bearing of backscattering objects (targets) can be provided by the radar on the basis of the time between the transmission of a pulse and the reception of the signal and by noting the antenna azimuth and elevation at the instant the signal is received. Raindrops, snowflakes, and cloud droplets are distributed radar targets, characterized by the presence of many effective scattering elements that are simultaneously illuminated by a transmitter pulse. For a distributed target constituted by spherical raindrops that are small with respect to the radar wavelength, the average power $\bar{P}_r$ received from a unit volume of rain-filled atmosphere at range r is given by

$$\bar{P}_r = c\,k\,Z/r^2, \tag{1}$$

where c is a constant involving radar parameters (e.g., wavelength, transmitted power, antenna gain, beam width, and pulse length), k is the fractional reduction in the signal attenuation along the path of propagation, and Z is a reflectivity factor which is proportional to the quantity $\sum D^6$, where D is the raindrop diameter and the summation $\sum$ is extended over the unit atmospheric contributing volume. This reflectivity factor can be expressed as

$$Z = \int_0^\infty N(D)\,D^6\,dD, \tag{2}$$

where $N(D)$ is the drop-size distribution, which expresses the number of raindrops per unit size of diameter D per unit volume of space.

When a value of Z is deduced from measured values of $\bar{P}_r$ by applying equation (1), it is called "equivalent radar reflectivity factor" and is designed by Z_e. The accuracy of the measured value of Z_e depends on knowledge of quantities in (1) [*Austin*, 1987]. The "equivalent rainfall intensity" R_e (or radar rainfall intensity) can be obtained from measured values of Z_e by using a Z-R relationship, which is an empirical relation between radar reflectivity factor Z and rainfall intensity R in a volume of air. Such relationships have been deduced by a number of scientists from measurements of drop-size distributions in natural rain [*Battan*, 1973]. For a Marshall-Palmer (MP) distribution of raindrops, $N(D) = N_0 e^{-\Lambda D}$, where the slope factor Λ, in centimeters to the power of -1, depends only on rainfall intensity R, in millimeters per hour, as given by $\Lambda = 41\,R^{-0.21}$, and the intercept parameter is a constant given by $N_0 = 0.08$ cm^{-4}; the reflectivity factor Z can be expressed as $Z = 6!\,N_0/41^7\,R^{1.47}$. The general form of this equation, as given by

$$Z = a\,R^b, \tag{3}$$

where a and b are constants, is known in the literature as MP Z-R relationship [*Marshall and Palmer*, 1948]. Values $a = 200$ mm^{6-b} m^{-3} and $b = 1.6$ in (3) generally provide reasonable approximations of the observed data for Z and R [*Rogers and Yau*, 1989]. Although several detailed studies have demonstrated that the MP raindrop distribution $N(D)$ is not sufficiently general to describe many observed raindrop spectra [*Pruppacher and Klett*, 1978] and that parameters a and b may vary significantly with rainfall type even in the same event [*Atlas et al.*, 1999], the relationship $Z = 200\,R^{1.6}$ is assumed in this work as standard descriptor of the Z-R relationship in a simple power function form. The question whether Z-R relationships, based on drop samples which represent only a few cubic meters of air, are applicable to radar measurements whose samples contain a number of cubic kilometers have been considered by *Austin* [1981]. She simulated more extensive spatial samples for the disdrometer by averaging data over periods of 5 min or less. She concluded that Z-R relationships from disdrometer data should apply for radar measurement cells of 4 km or less in dimension.

In this work, attention is focused on the relationship between radar reflectivity data and rainfall intensity at the land surface observed by rain gages. In this context, radar data of the equivalent reflectivity factor Z_e are assumed to be representative of the reflectivity factor Z, and equivalent rainfall intensity R_e reproduced from radar data is assumed to represent the rainfall intensity R. To simplify notations, the reflectivity factor is denoted by Z (instead of Z_e) also when measured by radar, and rainfall intensity is denoted by R (instead of R_e) also when obtained from radar data. Three-dimensional coverage of the radar echo and of the related estimates of the reflectivity factor Z are obtained by a programmed antenna scan, in which azimuth and elevation are systematically varied to survey all or most of the space around the radar site. Radar data are dis-

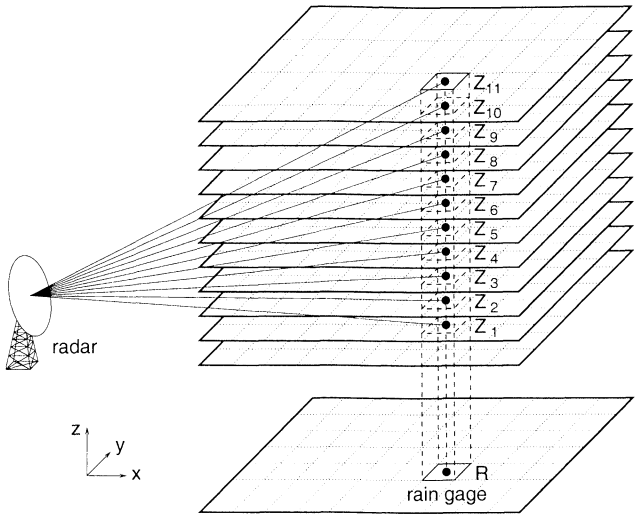

Figure 1. Sketch of the radar coverage of the atmospheric volume above the area where rainfall estimates are sought.

played on plan position indicators (PPIs), which map the received signals on polar coordinates on a plan view, or to constant altitude PPIs (CAPPIs), which map at several levels above the ground. The radar data processed in this work are obtained from a sequence of volumetric scans of the atmosphere above the study area and are collected in sets of 11 CAPPI images piled up for each time interval of the observation period (Figure 1). The radar signal is averaged in space and time to provide values of Z with spatial resolution of 2 km $\times$ 2 km $\times$ 1 km (along the x, y, and z coordinates of the Cartesian system) and with a time resolution of 15 min. The best relationship between vectors of radar reflectivity $\mathbf{Z}^T = (Z_1, \cdots, Z_{11})$ along the 11 CAPPI levels in the vertical atmospheric profile and the corresponding values of rainfall intensity at the land surface R is sought by training ANN models with observations of $\mathbf{Z}$ and R at each rain gage location in the study area and for each time interval of the observation period.

There are several remarks on the proposed strategy that ought to be expressed. ANN models are used to identify the relationship between radar reflectivity data mapped onto Cartesian volumes and rain gage measurements. This relationship may include possible influences related to radar operation, rainfall variability, and differences in radar/gage sampling (such as those mentioned in section 1) which could be corrected, at least in part, by means of physically based procedures. However, the significance of the proposed strategy is connected to the possibility of mapping directly radar reflectivity observations and rain gage measurements, filtering in some unknown way the noise and the bias in the data. The challenge of ANN modeling is to prove their ability to learn distributed nonlinear functional relationships from raw data sets which incorporate (explicitly or not) all the essential factors involved in the process of interest. Reflectivity data mapped onto Cartesian volumes are processed from original polar data, and this results in a loss of information with respect to original data. However, Cartesian data allow consistency in the format of the ANN input variables for different planar cell locations and this justifies their use in this first work. The use of original polar data may be evaluated in future more complex formulations. It is also remarked that the work described in this paper does not attempt to provide spatial patterns of ground level rainfall intensity directly as ANN output [e.g., *French et al.*, 1992]. Efforts are focused on the identification of a general relationship between observations of $\mathbf{Z}$ and R, which can provide the best possible estimates of R from observed $\mathbf{Z}$ at any given planar cell in the study area. Spatial statistical analysis of the obtained estimates of R is viewed as a next possible step [e.g., *Kavvas and Herd*, 1991; *Krajewski*, 1987; *Georgakakos and Krajewski*, 1991; *Bacchi et al.*, 1996].

2.2. ANN Architectures and Mappings

Three ANN models, namely a multilayer perceptron (MLP), a Bayesian network (BN), and a radial basis function network (RBFN), are used in this study to provide a nonparametric method for identifying the relationship between Z and R which is more robust to abnormal values and noise and which has more generalization capabilities than a standard MP relationship such as (3). These are three of the most widely used ANN models in applied statistics [*Bishop*, 1995; *Ripley*, 1996]. The general architecture of the selected ANNs is sketched in Figure 2. The selected ANN models have three fully connected layers, are feed forward in the sense that backpropagation of the signal is unidirectional, without feedback cycles between units, and are trained with supervision, namely presenting target values to the ANNs and minimizing a function of the quadratic error between predicted and desired values.

The MLP model is chosen to have a logistic transfer function from the input layer to the hidden layer and a linear transfer function from the hidden layer to the output layer. Useful approximation properties of a MLP having this kind of architecture are proven in the literature [*White*, 1989]. If one denotes the n-dimensional input vector by $\boldsymbol{x}^T = (x_1, \cdots, x_n)$ and the output variable by $y(\boldsymbol{x})$, then the MLP with $n+1$ input units

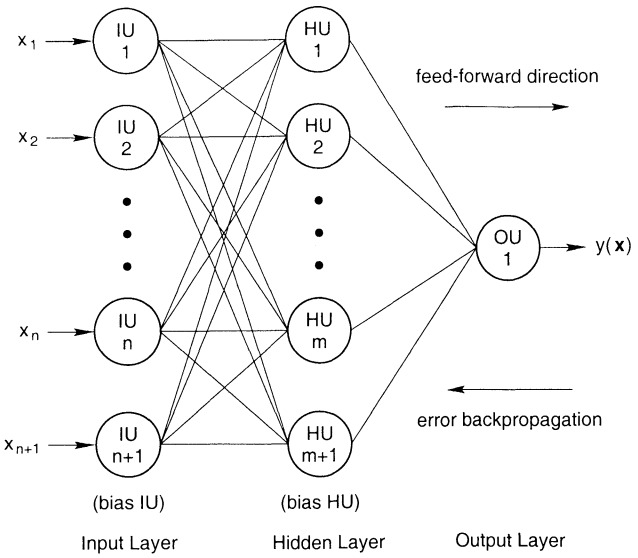

Figure 2. Architecture of a multilayered artificial neural network (ANN) with input layer constituted by $n+1$ input units (IUs), hidden layer constituted by $m+1$ hidden units (HUs), and output layer constituted by one output unit (OU). Note that there are $W = (n+2)(m+1)$ weights in this ANN.

(IUs), $m+1$ hidden units (HUs), and one output unit (OU) can be viewed as computing the nonlinear regression function

$$y(\boldsymbol{x}) = \sum_{j=1}^{m+1} w_j^{\mathrm{HO}} \mathcal{L}\left(\sum_{i=1}^{n+1} w_i^{\mathrm{IH}} x_i\right), \tag{4}$$

where $\mathcal{L}(\cdot)$ is the logistic function $\{1+\exp[-(\cdot)]\}^{-1}$, w_j^{HO} $(j=1,\cdots,m+1)$ are the weights connecting the hidden and the output layers, w_{m+1}^{HO} being the bias term to the output layer, and w_i^{IH} $(i=1,\cdots,n+1)$ are the weights connecting the input and the hidden layers, w_{n+1}^{IH} being the bias term to the hidden layer. The input value x_{n+1} is conventionally set equal to 1, so the product $w_{n+1}^{\mathrm{IH}} x_{n+1}$ provides a threshold for $\mathcal{L}(\cdot)$. Note that there are $W=(n+2)(m+1)$ weights in the considered ANN. Training (i.e., estimating the optimal values of the weights) is carried out through the minimization of the sum of squared errors between ANN predictions y_s $(s=1,\cdots,N)$ and corresponding target values t_s $(s=1,\cdots,N)$, given by

$$\varepsilon = \sum_{s=1}^{N} (y_s - t_s)^2, \tag{5}$$

N being the dimensionality of the training data set. A variety of approaches for minimizing this error function are possible, including standard optimization techniques such as Newton-type methods. For a discussion of possible computing strategies the reader is referred to *Nychka et al.* [1992] and *White* [1992]. In this work, backpropagation with the conjugate gradient algorithm is used, which involves calculating an approximation of the second derivative of the error with respect to a weight [*Gill et al.*, 1981]. If one denotes by $\varepsilon_s = (y_s - t_s)^2$ the contribution to ε from the sth training example, then the change in a weight w_k $(k=1,\cdots,W)$ to be applied as correction is given by

$$\Delta_s w_k = \frac{\partial \varepsilon_s / \partial w_k}{\partial^2 \varepsilon_s / \partial w_k^2}. \tag{6}$$

Overfitting (i.e., the fitting of noise in the data set) is controlled by means of the stopped training procedure. Training is stopped when no more sensible improvement in performance is found, which is when the variation of ε is negligible with proceeding of time, or when overfitting starts, which is when the test error ($\sum(y_s - t_s)^2$ on the test set) starts rising even if the training error ($\sum(y_s - t_s)^2$ on the training set) is still decreasing [*Bishop*, 1994; *Haykin*, 1995].

The BN model is a MLP with a logistic transfer function in the hidden layer and a linear transfer function in the output layer, trained to minimize a cost function C in which a penalty term is added to the error, in order to reduce the impact of noise, to penalize large weights, and to encourage smooth mapping functions. The Bayesian approach is implemented in this study by considering a weight decay penalty term and minimizing the cost function

$$C = \sum_{s=1}^{M} (y_s - t_s)^2 + \lambda \sum_{k=1}^{W} w_k^2, \tag{7}$$

where M is the dimensionality of the entire data set (number of available patterns) and λ is the regularization parameter. The Bayesian theory is particularly attractive since it allows the ANN to generalize without requiring the use of test data. All the M ($\gg N$) available patterns can therefore be used in the training process [*Bishop*, 1995]. Note that if independence between training patterns and additive zero mean Gaussian noise are assumed, minimizing the cost function C is equivalent to maximize the posterior distribution of the weights $p(\boldsymbol{w}|\boldsymbol{t})$, $\boldsymbol{w}=(w_1,\cdots,w_W)$ being the weight vector and $\boldsymbol{t}^T=(t_1,\cdots,t_M)$ the data set. In this framework the parameter $1/\lambda$ is the variance of the multinormal prior distribution of the weight vector $p(\boldsymbol{w})$ [*Ripley*, 1994, 1996].

The RBFN activates the hidden layer on the basis of the distance between the input vector and a prototype vector. Unlike the MLP and the BN, the RBFN is not based on units that compute a nonlinear function of the scalar product of the input vector and a weight vector [*Broomhead and Lowe*, 1988; *Moody and Darken*, 1989]. The RBFN mapping is a linear combination of a set of m radial basis functions (RBFs), which takes the form

$$y(\boldsymbol{x}) = \sum_{j=1}^{m} w_j \phi_j\left(\|\boldsymbol{x} - \boldsymbol{\mu}_j\|\right) + w_{m+1}, \tag{8}$$

where $\boldsymbol{x}$ is the n-dimensional input vector with elements x_i $(i=1,\cdots,n)$, and $\boldsymbol{\mu}_j$ is the vector determining the center of RBF ϕ_j and has elements μ_{ij} $(i=1,\cdots,n; j=1,\cdots,m)$. In this work the distance $\|\boldsymbol{x}-\boldsymbol{\mu}_j\|$ is taken to be Euclidean and the RBF are chosen to be Gaussians; that is,

$$\phi_j\left(\|\boldsymbol{x} - \boldsymbol{\mu}_j\|\right) = \exp\left(-\frac{\|\boldsymbol{x}-\boldsymbol{\mu}_j\|^2}{2\sigma_j^2}\right), \tag{9}$$

where the standard deviation σ_j, also called smoothing parameter, determines the width of the HUs and their degree of overlapping. Training is usually carried out in two phases. The parameters $\boldsymbol{\mu}_j$ and σ_j are first estimated through unsupervised procedures $(j=1,\cdots,m)$. The weights w_j $(j=1,\cdots,m+1)$ are then determined by linear optimization techniques [*Bishop*, 1995]. In this work the values of RBF centers $\boldsymbol{\mu}_j$ are sampled from the input training patterns and the number of RBF centers is determined by subset selection [*Morlini*, 1999]. The procedure starts with an empty subset to which one RBF at a time is added. To decide when to stop adding further RBFs, the error in the test set is also monitored. Although the training error never increases as extra functions are added, the test error eventually stops decreasing and starts to increase as overfit sets in. This is the point at which to cease adding RBF centers to the ANN. Even though subset selection is a nonlinear algorithm, the computational requirement is relatively low. As it only sets the RBF centers, the width parameters are chosen using some other heuristics. To give a relatively smooth representation of the distribution of the training data, the width parameters are chosen to be equal and to be given by the average of the distances between each RBF center and its nearest neighbor.

It is remarked here that the ANN models developed in this work do not attempt to model the underlying random process that generates the data and that the weight parameters do not have substantive interpretations that might be used to validate the ANN approach (even if, for Bayesian ANNs, this is possible under the circumstances previously described [*Mackay*, 1992]). The analysis is nonparametric in the sense that no a priori assumption is made about the distribution of the data,

the spatial correlation, and the time dependencies. Unlike traditional statistical methods, ANNs do not require assumptions about the model form. It is stressed here that the significance of ANN modeling described in this work is especially connected to their possible ability to learn distributed nonlinear functional relationships from raw data sets which incorporate in some (not completely known) way all the essential factors involved in the process of interest.

3. Real Case Application

3.1. Data Set

The problem presented in section 2.1 is solved with the methodology described in section 2.2 for the real case of the June 12, 1997, storm event in the Cortina d'Ampezzo area (eastern Italian Alps). Reflectivity data provided by the Monte Grande radar (Teolo, Italy) and rainfall intensity measurements provided by the five rain gages at the Passo Falzarego, Podestagno, Cortina d'Ampezzo, Faloria, Misurina sites are used. The five rain gage stations are distributed over a rectangular area of about 19 km × 8 km (along the x and y coordinates of the Cartesian system, respectively, Figure 1), and the average elevation of these stations is about 1731 m above sea level (asl). Rain gages are of the tipping bucket type with each flip-flop motion corresponding to 0.2 mm of precipitation. Rainfall intensity is measured at these five rain gages with a time resolution of 5 min. The Monte Grande radar operates in C-band with a 5.5-cm wavelength, linear horizontal polarization, beam width at 3 dB of 0.9°, peak power of 250 kW, quantization of 256 levels, possible elevations of 0°30′, 1°, 1°30′, 2°30′, 3°30′, 4°30′, 6°, 7°30′, 10°, and 15°, and maximum range in no-Doppler mode of 240 km [*Monai et al.*, 1994]. The distance between the centroid of the study area and the Monte Grande radar is about 138 km. At such a distance the Monte Grande radar operates only in no-Doppler mode, providing reflectivity data at 11 CAPPI levels with a space resolution of 2 km × 2 km × 1 km (along the x, y, and z coordinates of the Cartesian system, respectively, Figure 1) and time resolution of 15 min. The elevation of the radar is about 476 m asl and the CAPPI images of reflectivity at level zero (at 972 m asl) does not provide observations above the study area. Available CAPPI images range from level 1 (at 1972 m asl) to level 11 (at 11,972 m asl). Radar data collected by the agency responsible for the Monte Grande radar (Centro Meteorologico di Teolo, Teolo, Italy) are processed when they are converted to Cartesian data so as to control the effects of ground clutter, shielding, beam height, and beam width. The procedures employed are described by *Monai et al.* [1994]. Note that the extent and the efficiency of these procedures can hardly be evaluated by a radar data user, and this provides a further possible motivation for the use of the ANN modeling described in this paper. ANNs do not require assumption on the form of noise and bias and thus they should adapt to any (meaningful) available information.

The average cumulative rainfall depth recorded at the five rain gages during the June 12, 1997, storm event, from 1115 to 2400, is about 13 mm. To allow the comparison between rain gage and radar data, the 5-min resolution rainfall intensities measured by the rain gages are averaged over the same 15-min time intervals in which the radar observations are provided. The obtained values of R are coupled with the observations of radar reflectivity along the 11 CAPPI levels $\mathbf{Z}^T = (Z_1, \cdots, Z_{11})$ corresponding to the radar cells containing the rain gages and to the same time intervals. The monitoring of the June 12, 1997, storm event, from 1115 to 2400, in the Cortina d'Ampezzo area, provides a sample of $M = 255$ observations of R and $\mathbf{Z}$, each one of them being related to one of the 51 time intervals of 15 min that compose the observation period and to one of the 5 rain-gage/radar-cell locations. Descriptive statistics of the obtained data set are reported in Table 1. Note that the same values of Z appear at different adjacent CAPPI levels. This is due to excessive beam broadening at the considered radar-to-gage distances, which results in inadequate PPI volume resolution to provide different values of Z at each CAPPI level. From the shape of the Z profile along the vertical it is also revealed that no bright band caused by an anomalous return from a melting layer occurs during the summer storm considered in this work.

Table 1. Descriptive Statistics of Rain Gage Measurements R (in mm h^{-1}) and Radar Observations Z_i ($i = 1, \ldots, 11$) at the 11 CAPPI Levels (in $mm^6\ m^{-3}$)

Variable	Min	Max	Mean	s.d.
R	0	53	1	4
Z_1	0	275,422	3029	18,098
Z_2	0	275,422	3029	18,098
Z_3	0	91,201	1958	7789
Z_4	0	25,118	417	1962
Z_5	0	25,118	417	1962
Z_6	0	15,848	167	1064
Z_7	0	15,848	167	1064
Z_8	0	1318	27	91
Z_9	0	1318	20	87
Z_{10}	0	1318	14	84
Z_{11}	0	47	1	4

Min, minimum value; max, maximum value; mean, mean value; s.d., standard deviation.

As shown in Figure 3a, the MP relationship $Z = 200\,R^{1.6}$ provides a poor interpretation for the observed data of R and Z_1 at the five rain gage locations in the study area. Note that the number of points in Figure 3a is much less than the number of patterns in the data set $M = 255$, as for many of the time intervals in the observation period the rainfall intensity recorded at the five rain gages is zero. Radar rainfall estimates $R = (Z_1/200)^{1/1.6}$ obtained from the above MP relationship are compared with rain gage measurements at the Faloria Station, where the highest rainfall peak (53.6 mm h^{-1} over a 15-min interval) and cumulative depth (about 38 mm) are recorded (Figure 3b). The MP output appears rather nonsmooth and tends to overestimate near-zero measurements of R. Note that the MP relationship used in this work does not represent the limit of traditional (not based on ANNs) methods employed in radar meteorology, but it simply serves to express the performance of a procedure commonly employed in operational hydrology.

3.2. Principal Component Analysis

5

The spatial variability of Z along the 11 available CAPPI levels is explored by applying a principal component (PC) analysis over the standardized values of Z_i ($i = 1, \cdots, 11$), given by

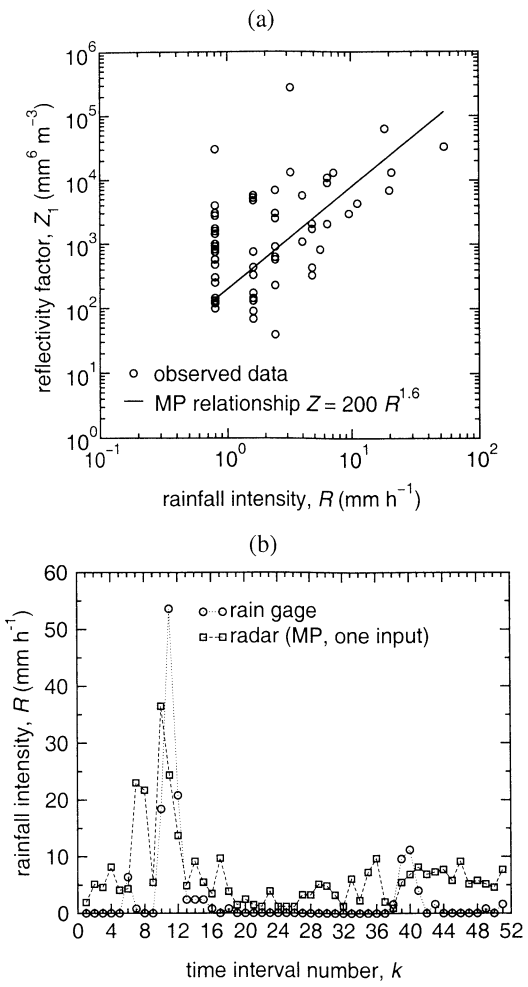

Figure 3. (a) Interpretation of the relationship between rainfall intensity measurements $R(>0)$ at the five considered rain gages and the corresponding reflectivity observations Z_1 at the lowest available constant altitude plan position indicator (CAPPI) level (level 1) with the Marshall-Palmer (MP) relationship $Z = 200\,R^{1.6}$. (b) Comparison between rain gage measurements and radar estimates of R at the Faloria site, during the June 12, 1997, storm event. Radar rainfall is obtained from the above MP relationship solved for R, namely $R = (Z/200)^{1/1.6}$, Z being set equal to Z_1.

$\tilde{Z}_i = (Z_i - E[Z_i])/\sqrt{\mathrm{Var}[Z_i]}$, where $E[Z_i]$ and $\mathrm{Var}[Z_i]$ denote the sample mean and variance of Z_i $(i = 1,\cdots,11)$, respectively. Standardized variables $\tilde{Z}_i$ $(i = 1,\cdots,11)$ have zero mean and unit variance. Standardization appears necessary due to the different ranges displayed by the Z_i values $(i = 1,\cdots,11)$ at the 11 CAPPI levels (Table 1). The PC analysis of the sample of standardized observations $\tilde{\mathbf{Z}}_s^T = (\tilde{Z}_1,\cdots,\tilde{Z}_{11})_s$ $(s = 1,\cdots,M)$ is geometrically carried out in an 11-dimensional space by translating the origin of the swarm of points at the sample mean vector (this has no effect for standardized data as $E[\tilde{\mathbf{Z}}] = 0$) and by rotating the $\tilde{Z}_i$ axes $(i = 1,\cdots,11)$ to line up with the natural extensions of the system of observations, so the dimension along which the observations are maximally separated or spread out is achieved [*Jolliffe*, 1986]. If $\boldsymbol{S}_{\tilde{\mathbf{Z}}}$ denotes the sample covariance matrix of $\tilde{\mathbf{Z}}$, with elements $(\boldsymbol{S}_{\tilde{\mathbf{Z}}})_{ij}$ given by $\mathrm{Cov}[\tilde{Z}_i, \tilde{Z}_j] = \sum_{s=1}^{M} (\tilde{Z}_i)_s (\tilde{Z}_j)_s / M$ $(i = 1,\cdots,11; j = 1,\cdots,11)$, and $\boldsymbol{e}_i$ $(i = 1,\cdots,11)$ is the normalized (i.e., $\boldsymbol{e}_i^T \boldsymbol{e}_i = 1$) eigenvector of $\boldsymbol{S}_{\tilde{\mathbf{Z}}}$ associated with the ith largest eigenvalue of $\boldsymbol{S}_{\tilde{\mathbf{Z}}}$, the PCs of $\tilde{\mathbf{Z}}$ are the transformed variables $\mathrm{PC}_1 = \boldsymbol{e}_1^T \tilde{\mathbf{Z}}$, $\mathrm{PC}_2 = \boldsymbol{e}_2^T \tilde{\mathbf{Z}}, \cdots, \mathrm{PC}_{11} = \boldsymbol{e}_{11}^T \tilde{\mathbf{Z}}$. Principal components are uncorrelated and reflect the directions (those of the eigenvectors $\boldsymbol{e}_i$ $(i = 1,\cdots,11)$ of $\boldsymbol{S}_{\tilde{\mathbf{Z}}}$) of maximum variance (given by the corresponding ith eigenvalues of $\boldsymbol{S}_{\tilde{\mathbf{Z}}}$). The score of the ith PC for the sth observation is $(\mathrm{PC}_i)_s = \boldsymbol{e}_i^T (\tilde{\mathbf{Z}})_s$ $(i = 1,\cdots,11; s = 1,\cdots,M)$. If some of the eigenvalues of $\boldsymbol{S}_{\tilde{\mathbf{Z}}}$ are small with respect to the others, we can neglect them and represent the data points in the lower q-dimensional representation spanned by the q eigenvectors associated to the q largest eigenvalues of $\boldsymbol{S}_{\tilde{\mathbf{Z}}}$. This representation is the most accurate rank-q reconstruction of the original swarm of points, since it minimizes the sum of squares of the distances from the data points to their projections into the space. For a synthetic but comprehensive discussion of the properties of the lower q-dimensional space spanned by the first q PCs the reader is referred, for instance, to *Ripley* [1996]. A recent discussion on the applicability of the PC analysis to geophysical data is provided by *Chung and Nigam* [1999].

The optimal number of PCs to be retained in order to efficiently summarize the original data set is decided in this work by excluding the PCs whose eigenvalues are less than the average of the eigenvalues of $\boldsymbol{S}_{\tilde{\mathbf{Z}}}$, i.e., 1. As this average value is also the average variance of the individual variables $\tilde{Z}_i$ $(i = 1,\cdots,11)$, the selected criterion retains those PCs that account for more variance than the average for the variables [*Krzanowski*, 1990]. In the application reported in this paper the retained PCs are 2. As reported in Table 2, the first two PCs of $\tilde{\mathbf{Z}}$ (those corresponding to eigenvalues greater than unity) are found to describe the 91% of the original variance. This reveals that the effective dimensionality of the input space is far less than 11, and the observed reflectivity data can be conveniently represented to a high accuracy by projection onto the first two eigenvectors of $\tilde{\mathbf{Z}}$. As reported in Table 3, the first PC is highly correlated to the values of $\tilde{\mathbf{Z}}$ at the the first 10 CAPPI levels, which are themselves strongly correlated between each other, while the second PC is correlated to the values of $\tilde{\mathbf{Z}}$ at the 11th CAPPI level, which is uncorrelated with the values of $\tilde{\mathbf{Z}}$ at all the other CAPPI levels. This structure of correlations can perhaps be attributed, at least in part, to the problem of signal attenuation since the reflectivity factor of the 11th CAPPI level is always equal to zero for data recorded in Podestagno and Misurina, which are the farthest away from the radar station. The first two PCs of $\tilde{\mathbf{Z}}$, namely PC_1 and PC_2, are used as inputs for the ANN models, so as to incorporate the essential variability of Z along the vertical atmospheric profile without increasing too much the number of inputs (and the related

Table 2. Eigenvalues of $\boldsymbol{S}_{\tilde{\mathbf{Z}}}$ for the First Two PCs of $\tilde{\mathbf{Z}}$

PC	EV	PV	CPV
PC_1	8.86	0.81	0.81
PC_2	1.12	0.10	0.91

PC, principal component of the sample vectors $\tilde{\mathbf{Z}}$; EV, eigenvalue of the sample covariance matrix $\boldsymbol{S}_{\tilde{\mathbf{Z}}}$; PV, proportion of variance; CPV, cumulative proportion of variance.

Table 3. Correlations Between $\tilde{Z}$ Values at the 11 CAPPI Levels and First Two PCs of $\tilde{\mathbf{Z}}$

PC	$\tilde{Z}_1$	$\tilde{Z}_2$	$\tilde{Z}_3$	$\tilde{Z}_4$	$\tilde{Z}_5$	$\tilde{Z}_6$	$\tilde{Z}_7$	$\tilde{Z}_8$	$\tilde{Z}_9$	$\tilde{Z}_{10}$	$\tilde{Z}_{11}$
PC_1	0.98	0.98	0.86	0.89	0.89	0.97	0.97	0.93	0.97	0.95	0.12
PC_2	0.04	0.04	0.31	−0.17	−0.17	−0.06	−0.06	0.02	0.04	−0.08	0.97

number of weights). This is expected to mitigate the risk of overparameterization of the ANN models, allowing satisfactory estimates of R even for relatively small training sets. PC_1 can be viewed as an optimally weighted mean of the Z_i values along the lowest 10 CAPPI levels. PC_2 is included in the ANN inputs as it appears statistically relevant on the basis of the criterion mentioned above. It is remarked here that although the proportion of variance accounted for by each PC is evaluated (Table 2), it is not possible to evaluate a priori the effects of these PCs on the ANN output. Unlike for parametric methods, this evaluation could only be conducted experimentally.

3.3. ANN Modeling

ANN models with the kind of architecture sketched in Figure 2 and mapping properties described in section 2.2 are developed to identify and reproduce the functional relationship between $\mathbf{Z}$ (or some representative input for $\mathbf{Z}$) and R. In ANN modeling, one of the major operational problems is to build a model that is able to capture the complex underlying processes of the investigated phenomenon but which does not fit too much of the noise on the training data. This highlights the need to optimize the complexity of the model, in order to achieve the best generalization. A model that is too simple or too inflexible may produce excessive bias, while one with too much flexibility may produce excessive variance [*Bishop*, 1995]. The application considered in the present work also requires a subtle balance of the model complexity against the limited number of available training patterns. The model complexity can be varied by changing the number of HUs, in the MLP and BN cases, or by changing the number of RBF centers, in the RBFN case. Structural stabilization is implemented in this work by training a range of models having different parameters on a sample of $N = 128$ observations (randomly chosen among the $M = 255$ available) and comparing numerical results obtained on a sample of the remaining $M - N = 127$ test patterns. The neural connection package included in the SPSS software is used [*Recognition Systems Ltd.*, 1998]. Although the regularization parameter λ which controls the degree of smoothness of the Bayesian network mapping function is usually set by the user, the neural connection package does not allow the user to select a desired value for λ and automatically adapts both the parameter and the other weights during training.

Numerical experiments are carried out in this work to (1) assess the capabilities of the developed ANN models to provide more accurate estimates of R than a standard MP relationship, when the same input is used for the two formulations; (2) assess the influence of incorporating the spatial variability of Z_i along the vertical atmospheric profile ($i = 1,\cdots,11$) on the ANN estimation of R; and (3) assess the influence of incorporating the time variability of $\mathbf{Z}$ prior to a time interval for which the estimates are provided on the ANN estimation of R. Outcomes of these numerical experiments are expressed by reporting the results obtained from three input configurations (Table 4). The first of them assumes as ANN input only the value of reflectivity at the lowest available CAPPI level (level 1) at the time interval k ($k = 1,\cdots,51$) for which the estimate R^k is provided (one input, Z_1^k, $n = 1$ in Figure 2). This input configuration is the same used to provide radar rainfall estimates based on the MP relationship $R^k = (Z_1^k/200)^{1/1.6}$. The second input configuration assumes as ANN inputs the first two PCs of $\tilde{\mathbf{Z}}$ at the time interval k ($k = 1,\cdots,51$) for which the estimate R^k is provided (two inputs, PC_1^k and PC_2^k, $n = 2$ in Figure 2). The third input configuration assumes as ANN inputs the first two PCs of

Table 4. Input Configurations and Architectural Parameters of ANN Models

ANN Input Configuration	Functional Relationship	Optimal Number of HUs/RBF Centers		
		MLP	BN	RBFN
One input, namely the value of Z at the lowest available CAPPI level (level 1), at the time interval k ($k = 1,\cdots,51$) for which the estimate R^k is provided	$R^k = f\left(Z_1^k\right)$	3	2	5
Two inputs, namely the first two PCs of $\tilde{\mathbf{Z}}$ at the time interval k ($k = 1,\cdots,51$)	$R^k = f\left(PC_1^k, PC_2^k\right)$	5	6	6
Four inputs, namely the first two PCs of $\tilde{\mathbf{Z}}$ at the time intervals k and $(k-1)$ ($k = 8^a,\cdots,51$)	$R^k = f\left(PC_1^{k-1}, PC_2^{k-1}, PC_1^k, PC_2^k\right)$	2	4	7

Number of ANN inputs and of HUs/RBF centers are those denoted by n and m, respectively, in section 2.2 and Figure 2, bias units being not included.

[a]See explanation in section 3.3, last paragraph.

Table 5. RMSEs (in mm h^{-1}) of Rainfall Estimates With Respect to Rain Gage Measurements

Model	Training Set	Test Set
One Input (Table 4)		
MP relationship $R = (Z_1/200)^{1/1.6}$	3.94	9.35
MLP with 3 HUs	2.55	4.71
BN with 2 HUs	2.63	3.65
RBFN with 5 RBF centers	2.52	4.54
Two Inputs (Table 4)		
MLP with 5 HUs	1.51	3.78
BN with 6 HUs	1.39	2.00
RBFN with 6 RBF centers	2.03	2.88
Four Inputs (Table 4)		
MLP with 2 HUs	1.57	3.55
BN with 4 HUs	1.56	0.78
RBFN with 7 RBF centers	1.70	3.87

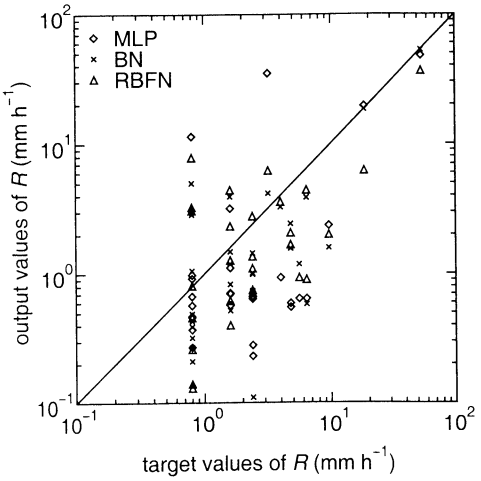

Figure 5. Test set target and output values of R, as obtained from the MLP, BN, and RBFN models with two inputs (Table 4).

$\tilde{\mathbf{Z}}$ at the time interval k ($k = 8, \cdots, 51$) for which the estimate R^k is provided and at the time interval $(k-1)$ immediately antecedent (four inputs, PC_1^{k-1}, PC_2^{k-1}, PC_1^k, and PC_2^k, $n = 4$ in Figure 2). Performances of the ANN models are expressed numerically, in terms of root-mean-square errors (RMSEs) for both the training and the test sets (Table 5), and visually, by plotting target and output values for the test set of R (Figures 4, 5, and 6, for one, two, and four ANN inputs, respectively), and by comparing the time series of rain gage measurements and ANN radar rainfall estimates at the Faloria Station during the considered storm event (Figures 7, 8, and 9, for one, two, and four ANN inputs, respectively).

In the first set of numerical experiments the optimal number (m in section 2.2) of HUs/RBF centers is empirically determined for ANN models with one input (Table 4). The MLP and BN are trained varying m and keeping weights initialization and all the other network parameters fixed. Ranging the number of HUs from 2 to 10, the best performances in terms of RMSE on the test set are obtained for a MLP with three HUs (RMSE of 4.71 mm h^{-1}) and for a BN with two HUs (RMSE of 3.65 mm h^{-1}, calculated over the 127 test patters in order to have comparable results). The optimal number of RBF centers in the RBFNs trained with subset selection is found to be 5 (RMSE of 4.54 mm h^{-1} on the test set). Table 5 reports the RMSEs on both the training and the test sets, for the MLP, BN, and RBFN models, as well as for the MP relationship $R = (Z_1/200)^{1/1.6}$ (where distinction between training and test sets of data is maintained to allow models comparison). ANNs clearly show useful gains over the MP relationship, which produces a RMSE equal to 9.35 mm h^{-1}. Although the RMSE is an expressive indicator of the overall agreement between measured and reproduced values of R, a more comprehensive comparison between rain gage measurements and radar estimates of R should also focus on the aptitude of the ANN mapping functions to reproduce rainfall peaks, which are the most im-

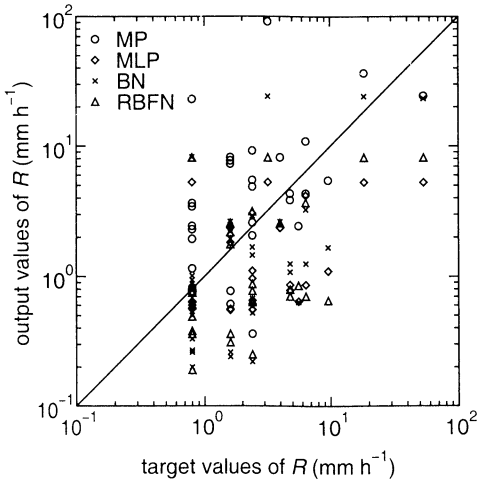

Figure 4. Test set target and output values of R, as obtained from the MP, multilayer perceptron (MLP), Bayesian network (BN), and radial basis function network (RBFN) models with one input (Table 4).

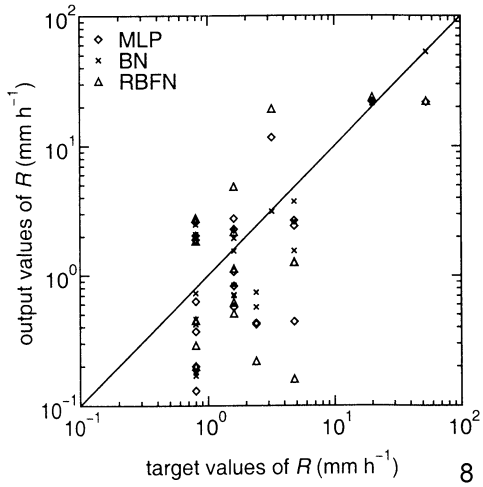

Figure 6. Test set target and output values of R, as obtained from the MLP, BN, and RBFN models with four inputs (Table 4).

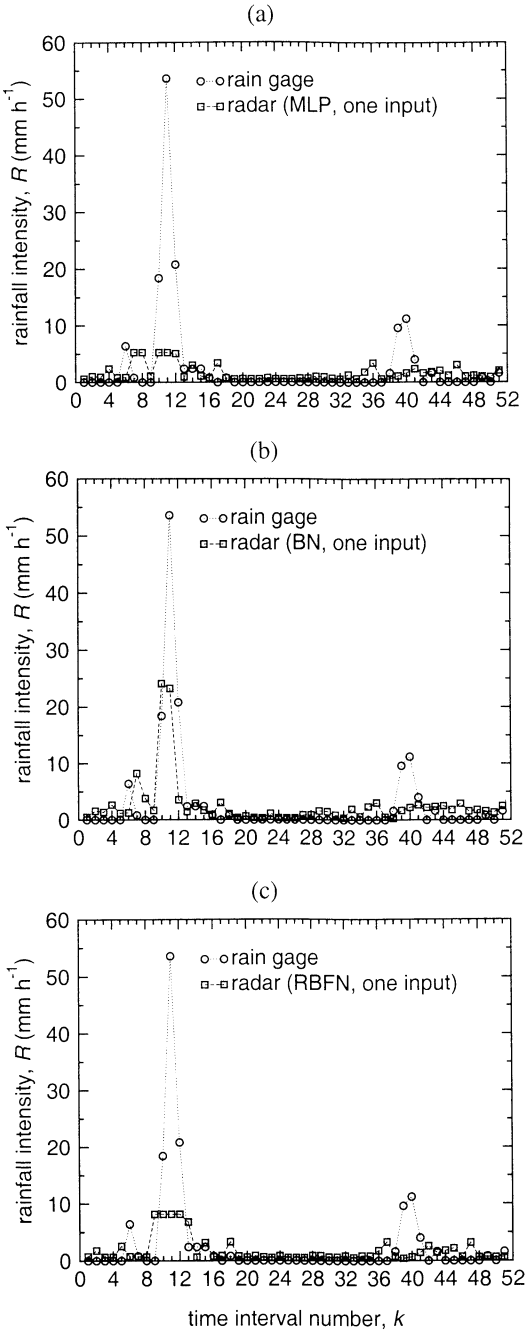

Figure 7. Comparison between rain gage measurements and radar estimates of R at the Faloria site, during the June 12, 1997, storm event. Radar rainfall is obtained using the MLP (a), BN (b), and RBFN (c) models with one input (Table 4).

portant to predict for the description of storm flows in natural drainage systems. This aptitude is visually tested by plotting the 15-min resolution rain gage measurements of R recorded at the Faloria Station, during the monitored storm event, along with the radar estimates of R provided by trained ANN models. Although these time series include values of R on both the training and the test sets (being the sets randomly composed), the major rainfall peaks are verified a posteriori to belong to the test set. Note that at the time resolution of 15 min, rainfall intensities greater than 10 mm h^{-1} may reasonably be considered as peaks. The results obtained from trained ANN models with one input are shown in Figures 4 and 7.

In the second set of numerical experiments the optimal number (m in section 2.2) of HUs/RBF centers is empirically determined for ANN models with two inputs (Table 4). The best numerical performances in terms of RMSE on the test set are obtained with five HUs for the MLP (RMSE of 3.78 mm h^{-1}) and with six HUs for the BN (RMSE of 2.00 mm h^{-1}). The optimal number of RBF centers in the RBFNs is found to be 6 (RMSE of 2.88 mm h^{-1} on the test set). As reported in Table 5 and shown in Figures 5 and 8, the performances reached by ANN models with the scores of the first two PCs of $\tilde{\mathbf{Z}}$ as input

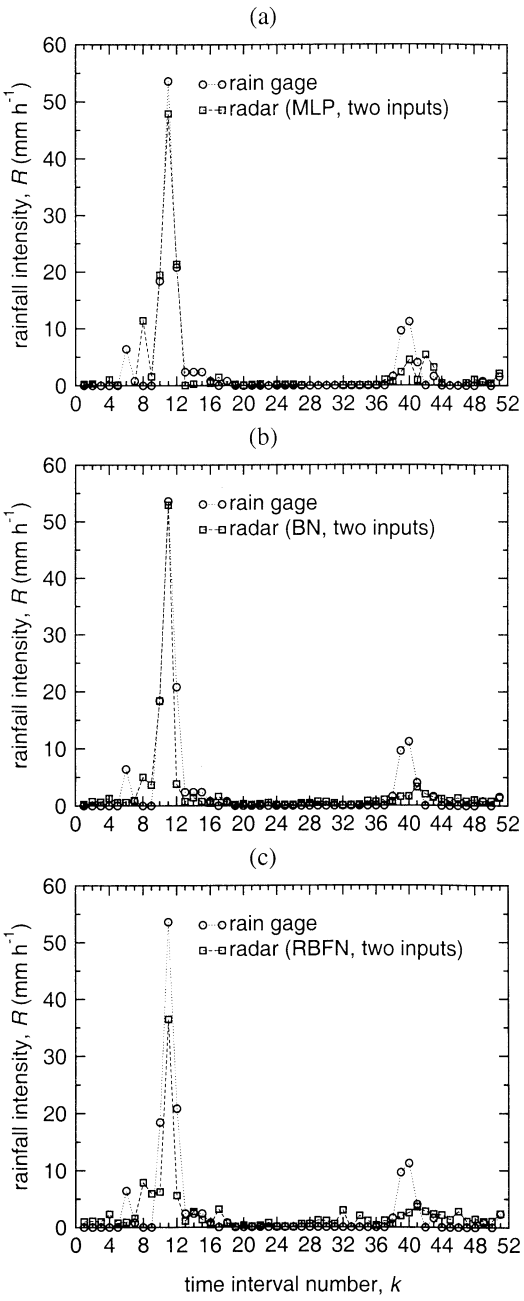

Figure 8. Comparison between rain gage measurements and radar estimates of R at the Faloria site, during the June 12, 1997, storm event. Radar rainfall is obtained using the MLP (a), BN (b), and RBFN (c) models with two inputs (Table 4).

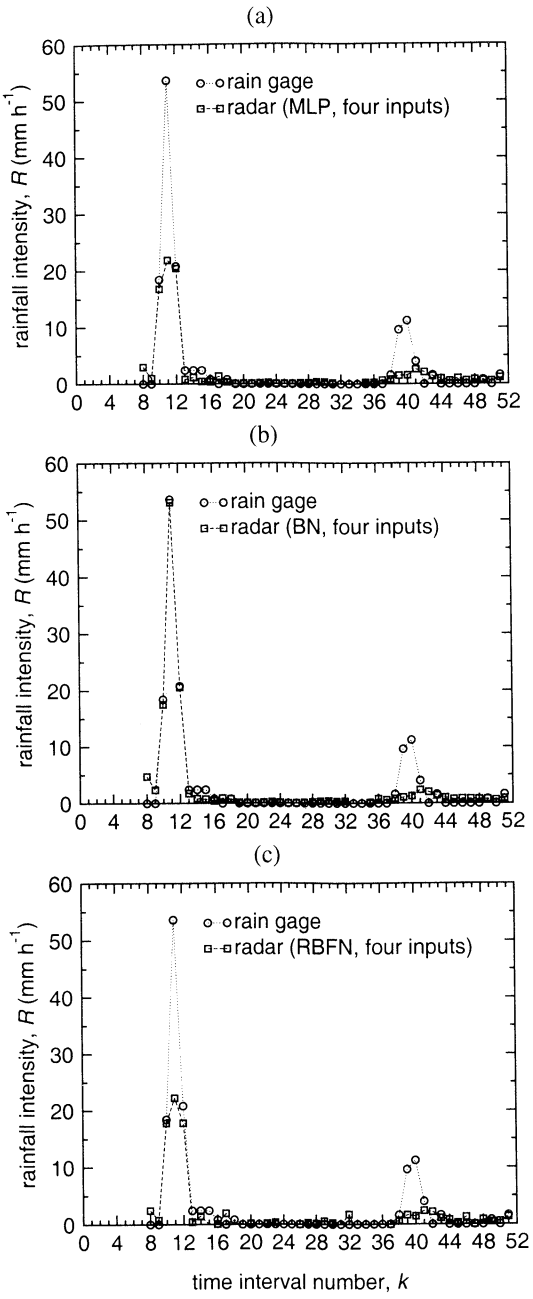

Figure 9. Comparison between rain gage measurements and radar estimates of R at the Faloria site, during the June 12, 1997, storm event. Radar rainfall is obtained using the MLP (a), BN (b), and RBFN (c) models with four inputs (Table 4).

variables are greatly improved with respect to those reached by ANN models with a single input.

In the third set of numerical experiments the influence of ANN inputs at the time intervals prior to the time interval k for which the radar estimates of R are provided is evaluated. Input vectors with 4, 8, 12, and 16 inputs, given by the scores of the first two PCs of $\tilde{\mathbf{Z}}$ at the last 2, 4, 6, and 8 time intervals prior to the kth (included), respectively, are used. Note that when variables at eight time intervals $(k-7,\cdots,k)$ are used in the ANN inputs, the first estimate of R is provided at the eighth time interval on the basis of the observations of Z at the first eight time intervals, and no estimates of R can be provided at the first seven time intervals. This implies that the first seven measurements of R at each rain gage cannot be considered to provide training or test patterns for the 16-input ANN models. These measurements are not considered also in the training and test sets for ANN models with 4, 8, and 12 inputs (even if part of them would be available) to allow ANN model results comparison. Only 220 of the 255 $(\mathbf{Z}, R)$ patterns are therefore used to train and test all the ANN models with lagged inputs. For any input configuration the optimal number (m in section 2.2) of HUs/RBF centers is empirically evaluated as carried out in the first two modeling steps described above. The results obtained reveal poor performances of all three ANN models increasing the number of inputs. The best results are obtained with the simplest model, the one with four inputs (namely the first two PCs of $\tilde{\mathbf{Z}}$ at the time intervals $(k-1)$ and k, Table 4). As reported in Table 5, these results are obtained from a MLP with two HUs (RMSE of 3.55 mm h^{-1} on the test set), from a BN with four HUs (RMSE of 0.78 mm h^{-1} on the test set), and from a RBFN with seven RBF centers (RMSE of 3.87 mm h^{-1} on the test set). From the above numerical results and from the comparison between Figures 8 and 9, it appears that the performances of the MLP and of the RBFN with four inputs are worsened with respect to those obtained in the case of two inputs, whereas the performances of the BN are improved and constitute the best simulation results obtained in this work.

4. Discussion

The analysis carried out in this work is meant to assess the capabilities of ANN models to identify the relationship between $\mathbf{Z}$ and R under critical operational circumstances, characterized by radar data of relatively low space-time resolution and poor quality, on the one hand, and by a limited number of rain gage measurements, on the other hand. These circumstances may be met in operational hydrology when the description of storm events is required over mountain areas with complex topography and long radar-to-gage distances, and where rain gages are sparse. As mentioned in the previous sections, the relation between observed radar reflectivity and surface rainfall is highly complex as it depends on a number of physical factors, the effect of which may vary significantly from one storm to another [*Austin*, 1987]. It appears therefore unrealistic to expect that a single Z-R relationship can be both sufficiently reliable to be useful and sufficiently general to be applied to all situations. The capabilities of ANN models to identify the relationship between $\mathbf{Z}$ and R are therefore evaluated, as a first step, considering a single storm event over a small geographical area, where the atmospheric and operational circumstances are expected to vary relatively little. As shown in Figures 3a, in the real case application considered in this work, the MP relationship $Z = 200\,R^{1.6}$ offers poor interpretation and prediction capabilities. The high values of the RMSEs reported in Table 5 and the visual comparison between rain gage and radar rainfall intensity shown in Figure 3b reveal a poor ability of a simple MP formulation even to identify storm and interstorm periods. Observed rainfall peaks are not well reproduced and significant values of radar rainfall intensity are generated when no rainfall is recorded by the rain gage.

As shown in Figures 4 and 7, ANN models with one input do not provide more accurate estimates of rainfall peaks than the MP relationship but display an improved capability to rec-

ognize storm and interstorm periods, and this results in smaller values of RMSEs in Table 5 with respect to those provided by the MP relationship. The incorporation of the essential features of the vertical profile of Z in the ANN models with two inputs is shown in Figures 5 and 8 to improve significantly the agreement between rain gage measurements and radar rainfall estimates for both the description of rainfall peaks and the identification of storm and interstorm periods, and this results in relatively small values of RMSEs in Table 5. The incorporation of the time variability of Z prior to the interval at which the estimates of R are provided produces different effects on the performance of the ANN models. The estimation capabilities of the MLP and RBFN models with four inputs (Figures 9a and 9c, respectively) are found to worsen with respect to the capabilities displayed in the case of two inputs (Figures 8a and 8c, respectively), whereas the estimation capabilities of the BN models with four inputs (Figures 9b) are found to improve with respect to the case of two inputs (Figures 8b), leading to the best simulation results obtained in this work (Table 5). This behavior of the considered ANN models may likely be due to the inability of the MLP and RBFN models to recognize and reproduce complex patterns with small training sets. The robustness of the BN models to such circumstances may be connected to the possibility for them to use the entire data set in the training process. As mentioned in section 2.2, the BN avoids overfitting by means of a penalty term in the cost function (7), and this makes unnecessary the stopped training procedure and the related division of the data set into training/test sets. The possibility of using the entire data set in the training process allows the BN to handle more inputs than the MLP and the RBFN.

Comparison between ANN models reveals that the BNs generally provide the lowest RMSE and the most accurate fits for peak values of R. This is likely to be due to the larger training set used for specifying a mapping function with generalization capabilities and is particularly relevant in the case of four inputs, where the largest parameter set needs to be determined. The possibility of using the entire data set in the case of the BNs is therefore shown to be a crucial factor, which leads to best performance of the BNs with respect to the other ANN models for any given input configuration, on the one hand, and to the possibility of taking advantage of complex input configurations, on the other hand. These propositions must be qualified by the fact that particular atmospheric circumstances are considered in this work and a limited data set is used. In particular, on a limited data set, the (random) selection of the training and test set may have a significant influence on the obtained scores. Values of RMSE in Table 5 related to the MP relationship seems to indicate that the test set is not easier to be interpreted (RMSE 9.35 mm h^{-1}) than the training set (RMSE of 3.94 mm h^{-1}) and thus the performance of the ANN models on both training and test sets are likely to reflect the capabilities of these models to learn and reproduce the relationship between Z and R, respectively. RMSEs related to the ANN model simulations are all greater for the training set than for the test set except for the case of the BN model with four inputs, and this may perhaps indicate a particularly favorable computational circumstance. A cross-calibration procedure (where several divisions of the data set into training/test sets are considered) could be useful to reduce the dependence of results on the division of the data set.

Possible physical interpretations of the results reported above are provided here with reference to the different character of radar and rain gage measurements. As discussed by *Zawadzki* [1975], besides random error, bias in the radar-gage comparison is introduced mainly by two factors. On the one hand, postdetection integration of Z over large atmospheric volumes (2 km × 2 km × 1 km in this study) results in spatially smoothed radar rainfall estimates, which are hardly comparable with punctual rain gage measurements. On the other hand, observations of Z at considerable height (up to 10 km in this study) above the ground contribute to rainfall estimates at the land surface with a significant time delay. Spatial smoothing and time lag between radar reflectivity and rain gage measurements lead to systematic underestimation of rainfall peaks and overestimation of low rainfall intensities. These effects are noticed in the real case application examined in this study, when using a standard MP relationship (Figure 3b). Identification and correction of the above mentioned bias by ANN models may constitute, at least in part, a possible explanation of the improvement in the ANN rainfall estimates with respect to those provided by the MP relationship. These presumed ANN capabilities appear less useful when one input is used (Figure 7) but become more effective, at least for the BN models, when values of Z at different altitudes and time intervals are incorporated in the ANN inputs (Figures 8 and 9).

5. Conclusions

Numerical experiments carried out in this work revealed that ANN models may play an important role in the identification and reproduction of the relationship between Z and R, even when they are trained on a relatively small data set obtained from the monitoring of a single storm event (51 time intervals of 15 min) over a small geographical area with a normal rain gage density (19 km × 8 km, with five rain gages). Even when the same one input (Table 4) was used for both the standard MP relationship and the ANN models, the latter were found to produce smoother mapping functions, which provide satisfactory estimates of near-zero target values without ignoring rainfall peaks (Figure 7), resulting thus in smaller RMSEs (Table 5). Additional improved capabilities of the ANN models appear to be connected to the possibility of incorporating the spatial variability of Z along the vertical atmospheric profile (Figure 8, Table 5). In this regard, the PC analysis was found to offer an efficient tool for synthesizing the values of Z along the 11 available CAPPI levels into two orthogonal inputs (Table 4) for the ANN models. The incorporation of the time variability of Z, during the time intervals prior to the interval for which the estimates of R are provided, highlighted the crucial problem in the ANN modeling addressed in this work, namely the need to maintain a balance between adaptive parameters and training observations. The use of four inputs (Table 4) for the ANN models led to further improvement in the performance of the BN (Figure 9b, Table 5) but led to worsened performance with respect to the case of two inputs (Table 4) for the other two networks (Figures 9a and 9b, Table 5), which appeared more sensible than the BN against the overparameterization risk (Figures 4, 5, and 6). In the application described in this paper, overfitting and overparameterization (which are two of the major areas of concern for the practical use of ANNs) appear to

be connected to each other, and the BN appears less vulnerable to these factors than the MLP and the RBFN.

The results obtained in this work must be qualified by the facts that they refer (1) to a single storm event, characterized by particular atmospheric circumstances (e.g., no signal enhancement by melting snow is observed) and (2) to particular operational circumstances (radar operation over very rugged terrains with long radar-to-gage distances). Although a more comprehensive validation is needed for the developed formulation, the combined use of PC analysis and BN models appears to constitute a new efficient statistical methodology for the estimation of rainfall intensity at the land surface from radar observations. Future work is encouraged in order to investigate the effects on the ANN estimation of R of training (1) on more than one storm event of the same nature, under similar operational circumstances; (2) on more than one storm event of different nature, under similar operational circumstances; and (3) on more than one storm event of different nature, under different operational circumstances. These modeling steps are required to assess the possible extension of the developed methodology for rainfall intensity estimation over large areas. The key problem connected to this possible extension is to identify and efficiently incorporate in the ANN inputs all the necessary factors that allow ANN models to recognize the variable circumstances produced by atmospheric processes and radar operation.

Notation

ANN artificial neural network.
a coefficient in the MP relationship, $\mathrm{mm}^{6-b}\ \mathrm{m}^{-3}\ \mathrm{h}^{b}$.
BN Bayesian network.
b exponent in the MP relationship, dimensionless.
CAPPI constant altitude PPI.
CPV cumulative proportion of variance.
c constant in equation (1) involving radar parameters.
D raindrop diameter, cm.
EV eigenvalue.
$\boldsymbol{e}_i$ ith eigenvector of $\boldsymbol{S}_{\tilde{\boldsymbol{Z}}}$ associated to the ith largest eigenvalue of $\boldsymbol{S}_{\tilde{\boldsymbol{Z}}}$, dimensionless.
HU hidden unit.
IU input unit.
k fractional reduction in the signal in (1); counter of time intervals, dimensionless.
$\mathcal{L}(\cdot)$ logistic functions, dimensionless.
M number of observed patterns $(\boldsymbol{Z}, R)$, dimensionless.
MLP multilayer perceptron.
MP Marshall-Palmer.
$m+1$ number of HUs (bias HU included), dimensionless.
N number of observed patterns $(\boldsymbol{Z}, R)$ used to train the MLP and the RBFN models, dimensionless.
$n+1$ number of IUs (bias IU included), dimensionless.
$N(D)$ drop-size distribution, cm^{-4}.
N_0 intercept parameter of $N(D)$, cm^{-4}.
OU output unit.
PC principal component.
PC_i ith PC of $\tilde{\boldsymbol{Z}}$, dimensionless.
PPI plan position indicator.
$\bar{P}_r$ average power received by the radar from a unit volume of atmosphere as given by (1).
PV proportion of variance.
R rainfall intensity at the land surface, $\mathrm{mm\ h}^{-1}$.
RBF radial basis function.
RBFN radial basis function network.
RMSE root-mean-square error.
r radar range.
$\boldsymbol{S}_{\tilde{\boldsymbol{Z}}}$ sample covariance matrix of $\tilde{\boldsymbol{Z}}$, dimensionless.
t target values for the ANN output variable y.
$\boldsymbol{t}$ vector of the values of t.
W number of weights in the considered ANN models, $W=(n+2)(m+1)$, dimensionless.
w weight in the ANN models, dimensionless.
$\boldsymbol{w}$ vector of the values of w.
x horizontal coordinate of the Cartesian system, m; generic ANN input variable.
$\boldsymbol{x}$ vector of the ANN input variable values of x.
y horizontal coordinate of the Cartesian system, m; generic ANN output variable.
Z reflectivity factor, $\mathrm{mm}^6\ \mathrm{m}^{-3}$.
$\boldsymbol{Z}$ vector of the values of Z along the vertical atmospheric profile, $\mathrm{mm}^6\ \mathrm{m}^{-3}$.
$\tilde{Z}$ standardized values of Z, dimensionless.
$\tilde{\boldsymbol{Z}}$ vector of the values of $\tilde{Z}$, dimensionless.
z vertical coordinate of the Cartesian system, m asl.
ε sum-square errors on y with respect to t.
ε_s contribution to ε from the sth training example.
ϕ RBF in the RNFN model, dimensionless.
Λ slope factor of $N(D)$, cm^{-1}.
λ regularization parameter in the BN model, dimensionless.
$\boldsymbol{\mu}$ vector of centers of the RBFs ϕ, dimensionless.
σ standard deviations of the Gaussian RBFs ϕ.

Acknowledgments. This research was jointly supported by the Ministero dell'Università e della Ricerca Scientifica e Tecnologica of Italy through the grant MURST Giovani Ricercatori "Analisi Distribuite degli Eventi di Piena" and by the European Community through the grant ENV4-CT96-0253 ("Debris Flow Risk" project, coordinated by Alberto Lamberti, Università degli Studi di Bologna, Bologna, Italy). The Centro Meteorologico di Teolo (Teolo, Italy) is gratefully acknowledged for providing radar and rain gage measurements used in this work. The authors thank Claudio Paniconi (CRS4, Cagliari, Italy) and three anonymous reviewers for comments that led to improvements in the manuscript.

References

Andrieu, H., and J. D. Creutin, Identification of vertical profiles of radar reflectivity for hydrological applications using an inverse method, part I, Formulation, *J. Appl. Meteorol.*, *34*, 225–239, 1995.

Andrieu, H., G. Delrieu, and J. D. Creutin, Identification of vertical profiles of radar reflectivity for hydrological applications using an inverse method, part II, Sensitivity analysis and case study, *J. Appl. Meteorol.*, *34*, 240–259, 1995.

Atlas, D., C. W. Ulbrich, F. D. Marks Jr., E. Amitai, and C. R. Williams, Systematic variation of drop size and radar-rainfall relations, *J. Geophys. Res.*, *104*, 6155–6169, 1999.

Austin, P. M., On deducing rainfall from radar reflectivity measurements, in *Proceedings 20th Conference on Radar Meteorology*, pp. 200–207, Am. Meteorol. Soc., Boston, Mass., 1981.

Austin, P. M., Relation between measured radar reflectivity and surface rainfall, *Mon. Weather Rev.*, *115*, 1053–1070, 1987.

Bacchi, B., R. Ranzi, and M. Borga, Statistical characterization of spa-

tial patterns of rainfall cells in extratropical cyclones, *J. Geophys. Res.*, *101*, 26,277–26,286, 1996.

Battan, L. J., *Radar Observation of the Atmosphere*, Chicago Univ. Press, Chicago, Il., 1973.

Bishop, C. M., Neural networks and their applications, *Rev. Sci. Instrum.*, *55*, 1803–1832, 1994.

Bishop, C. M., *Neural Networks for Pattern Recognition*, Clarendon, Oxford, England, 1995.

Brandes, E. A., Optimizing rainfall estimates with the aid of radar, *J. Appl. Meteorol.*, *14*, 1339–1345, 1975.

Broomhead, D. S., and D. Lowe, Multivariable functional interpolation and adaptive networks, *Complex Syst.*, *2*, 321–335, 1988.

Chagnon, S. A., and J. L. Vogel, Hydroclimatological characteristics of isolated severe rainstorms, *Water Resour. Res.*, *17*, 1694–1700, 1981.

Chung, C., and S. Nigam, Weighting of geophysical data in principal component analysis, *J. Geophys. Res.*, *104*, 16,925–16,928, 1999.

French, M. N., W. F. Krajewski, and R. R. Cuykendall, Rainfall forecasting in space and time using a neural network, *J. Hydrol.*, *28*, 121–126, 1992.

Georgakakos, K. P., and M. L. Kavvas, Precipitation analysis, modeling, and prediction in hydrology, *Rev. Geophys.*, *25*, 163–178, 1987.

Georgakakos, K. P., and W. F. Krajewski, Worth of radar data in the real-time prediction of mean areal rainfall by nonadvective physically based models, *Water Resour. Res.*, *27*, 185–197, 1991.

Gill, P. E., W. Murray, and M. H. Wright, *Practical Optimization*, Academic, San Diego, Calif., 1981.

Hanna, E., How effective are tipping-bucket raingauges?, A review, *Weather*, *50*, 336–342, 1995.

Haykin, S., *Neural Networks: A Comprehensive Foundation*, Macmillan, Indianapolis, Indiana, 1995.

Jolliffe, I. T., *Principal Component Analysis*, Springer-Verlag, New York, 1986.

Joss, J., and R. Lee, The application of radar-gauge comparisons to operational precipitation profile corrections, *J. Appl. Meteorol.*, *34*, 2612–2630, 1995.

Joss, J., and A. Pittini, Real-time estimation of the vertical profile of radar reflectivity to improve the measurement of precipitation in an Alpine region, *Meteorol. Atmos. Phys.*, *47*, 61–72, 1991.

Kavvas, M. L., and K. R. Herd, A radar-based stochastic model for short-time-increment rainfall, *Water Resour. Res.*, *21*, 1437–1455, 1991.

Krajewski, W. F., Cokriging radar-rainfall and rain gage data, *J. Geophys. Res.*, *92*, 9571–9580, 1987.

Krajewski, W. F., and J. A. Smith, On the estimation of climatological *Z-R* relationships, *J. Appl. Meteorol.*, *30*, 1436–1445, 1991.

Krzanowski, W. J., *Principles of Multivariate Analysis, A User's Perspective*, Clarendon, Oxford, England, 1990.

Mackay, D. J. C., A practical Bayesian framework for backpropagation networks, *Neural Comput.*, *4*, 698–714, 1992.

Marshall, J. S., and M. W. Palmer, The distribution of raindrops with size, *J. Meteorol.*, *5*, 165–166, 1948.

Monai, M., A. D. Pesci, and A. Trolese, Applications of advanced techniques at Monte Grande weather radar, *Tech. Rep.*, Cent. Sper. per l'Idrol. e la Meteorol., Teolo, Italy, 1994.

Moody, J., and C. J. Darken, Fast learning in networks of locally-tuned processing units, *Neural Comput.*, *1*, 281–294, 1989.

Morlini, I., Radial basis function networks for pattern recognition, Ph.D. thesis, Univ. degli Studi di Trento, Trento, Italy, 1999.

Nešpor, V., and B. Sevruk, Estimation of wind induced error of rainfall gauge measurements using a numerical simulation, *J. Atmos. Oceanic Technol.*, *16*, 450–464, 1999.

Nychka, D., S. Ellner, A. R. Gallant, and D. McCaffrey, Finding chaos in noisy systems, *J. R. Stat. Soc. London, Ser. B*, *54*, 399–426, 1992.

Pruppacher, H. R., and J. D. Klett, *Microphysics of Clouds and Precipitation*, D. Reidel, Norwell, Mass., 1978.

Recognition Systems Ltd., *Neural Connection 2.1*, SPSS Inc., Chicago, Il., 1998.

Ripley, B. D., Neural networks and related methods for classification (with discussion), *J. R. Stat. Soc. London, Ser. B*, *56*, 409–456, 1994.

Ripley, B. D., *Pattern Recognition and Neural Networks*, Cambridge Univ. Press, New York, 1996.

Rogers, R. R., and M. K. Yau, *A Short Course in Cloud Physics*, Pergamon, New York, 1989.

Steiner, M., J. A. Smith, S. J. Burges, C. V. Alonso, and R. W. Darden, Effect of bias adjustment and rain gauge data quality control on radar rainfall estimation, *Water Resour. Res.*, *35*, 2487–2503, 1999.

Troutman, B. M., Runoff prediction errors and bias in parameter estimation induced by spatial variability of precipitation, *Water Resour. Res.*, *19*, 791–810, 1983.

White, H., Some asymptotic results for learning in single hidden layer feed-forward network models, *J. Am. Stat. Assoc.*, *84*, 1003–1013, 1989.

White, H., *Artificial Neural Networks: Approximation and Learning Algorithms*, Blackwell, Malden, Mass., 1992.

Wilson, J. W., and E. A. Brandes, Radar measurements of rainfall, A summary, *Bull. Am. Meteorol. Soc.*, *60*, 1048–1058, 1979.

Xiao, R., and V. Chandrasekar, Development of a neural network based algorithm for rainfall estimation from radar observations, *IEEE Trans. Geosci. Remote Sens.*, *35*, 160–171, 1997.

Zawadzki, I. I., On radar-raingage comparison, *J. Appl. Meteorol.*, *14*, 1430–1436, 1975.

I. Morlini, Dipartimento di Economia, Sezione Statistica, Università degli Studi di Parma, Via Kennedy 6, I-43100 Parma, Italy.

S. Orlandini, Dipartimento di Ingegneria, Università degli Studi di Ferrara, Via Saragat 1, I-44100 Ferrara, Italy. (sorlandini@ing.unife.it)

(Received January 24, 2000; revised May 17, 2000;
accepted June 22, 2000.)